IEEE Access
Multidisciplinary | Rapid Review | Open Access Journal

Received 31 July 2024, accepted 28 August 2024, date of publication 2 September 2024, date of current version 10 September 2024.

Digital Object Identifier 10.1109/ACCESS.2024.3452763

RESEARCH ARTICLE

Optimizing the Durability of Buildings Against Earthquake-Induced Collapse by the Implementation of Deep Learning-Based Control Strategy

NORMAISHARAH MAMAT[1], RAWAD ABDULGHAFOR[2], (Member, IEEE), SHERZOD TURAEV[3], (Member, IEEE), FITRI YAKUB[4], (Senior Member, IEEE), AND MOHD FAUZI BIN OTHMAN[4]

[1]Faculty of Artificial Intelligence, Universiti Teknologi Malaysia, Kuala Lumpur 54100, Malaysia
[2]Faculty of Computer Studies (FVS), Arab Open University Oman, Muscat, Oman
[3]Department of Computer Science and Software Engineering, College of Information Technology, United Arab Emirates University, Al Ain, United Arab Emirates
[4]Department of Electronic System Engineering, Malaysia–Japan International Institute of Technology, University Teknologi Malaysia, Kuala Lumpur 54100, Malaysia

Corresponding authors: Rawad Abdulghafor (rawad.a@aou.edu.om) and Sherzod Turaev (sherzod@uaeu.ac.ae)

This work was supported in part by Sandooq Al Watan, United Arab Emirates, through United Arab Emirates University under SWARD Research under Grant G00003606 (21R092-PRJ-SWARD-510); in part by the Big Data Analytics Center, United Arab Emirates, under UAEU Strategies Research under Grant G00003606; and in part by Arab Open University Oman under the Internal Grant-Research Office and Universiti Teknologi Malaysia (Research Grant Professional Development Research University) under Grant Q.K130000.21A2.05E38.

ABSTRACT Natural disasters have the potential to inflict damage to building structures, which prompting the structural engineers striving to build buildings that are both safer and durable. This research endeavor aims to enhance the stability of a structure by using control strategy to reduce the hazards of earthquake-induced damage. As a consequence, a hybrid control device incorporates control strategies to improve structural integrity has been investigated. This study proposes control system comprising integrated nonsingular terminal sliding mode control (TSMC), nonsingular TSMC, and TSMC. Integrated nonsingular TSMC merges deep learning methods, specifically long short-term memory (LSTM). LSTM has the capability to forecast subsequently values by analyzing previous sequential data. This character enhances precision in systems, leading to better decision-making. This attribute enhances the precision of any system, contributing to better decision-making. The integration controller empowers the system to adjust its operation to achieve the most optimal mode of operation, hence improving control performance regardless of significant uncertainty. The integrated controller is invented using both the control law and sliding surface. A two-degree-of-freedom (DOF) system structure is constructed in Matlab and validated by experimental work associated with LMS Test.Lab software. In addition, the integrated controller is employed in a 10-DOF system represents a high-level structure. The performance of integrated nonsingular TSMC is compared to nonsingular TSMC and TSMC in terms of displacement response, sliding surface, and damage probability. The outcomes indicated that integrated nonsingular TSMC could mitigate vibration by up to 46% and had a 15% possible risk of inflicting complete damage to the controlled structure of a low-rise building. Its installation in high-rise structures resulted in the suppression of 26%. Consequently, these findings are crucial in enhancing the safety of building structures and residents, and minimizing disaster damage costs.

INDEX TERMS Deep learning, control strategy, earthquake control, building durability.

I. INTRODUCTION

An earthquake, as a natural event, poses a threat to lives, can lead to severe financial implications, and inflict significant

The associate editor coordinating the review of this manuscript and approving it for publication was Hassen Ouakad.

environmental damage. Significant earthquakes cause harm to buildings, property, and humans. Earthquakes killed many lives, but technological advances have significantly decreased the number of fatalities [1]. The method of suppressing structural building vibration in the event of an earthquake is becoming increasingly difficult. The cascade event on September 28, 2018, are typical of a devastating disaster scenario in which significant earthquakes are triggered, resulting in severe damages and losses. An earthquake with magnitude of 7.4 Mw, occurred in Sulawesi, Indonesia caused 68 451 structural damage, 2 100 deaths, and 4 612 injuries [2]. Once the magnitude of an earthquake achieved 5.0 Mw, the structure and buildings may experience minor damage. In a populated area, an earthquake of a magnitude greater than 6.0 Mw may causes extensive damage, and strong earthquakes with magnitudes of 7.0 Mw or higher also inflict significant damage. If the moment magnitude is more than 8.0 Mw, the community near the seismic location will be completely devastated [3].

There are around 20 earthquakes with a moment magnitude scale rating over 7.0 Mw per year. HAZUS is a tool for calculating the potential for seismic ground motion losses in the existing building stock. Through the Federal Emergency Management Agency (FEMA), HAZUS employs a geographic information system to assess the physical, economic, and social consequences of disaster preparedness strategies and building stock recovery methods [4]. Additionally, building curves for different types of structures are developed using HAZUS, which describes the information on the probability of damage states that include minor, moderate, extensive, and complete damage [5]. In general, there are four types of structural damage, comprising minor, moderate, extensive, and complete damage. Slight damage part occurs when small plaster cracks show up around window and door corners. In the moderate stage, larger fractures start to show in the corners of the windows and doors and the sheared wall panel. Large diagonal cracks are also created across the shear wall panel as a result of the extensive damage and the floors and ceiling are permanently laterally displaced. Finally, a complete damage state condition is evaluated when a major permanent lateral displacement or imminent threat of collapse is detected [6], [7]. Structural reliability is evaluated by defining fragility or vulnerability as the probabilistic risk of failure [8].

Fragility curves are produced from the fragility function, which reflects the probability of structural damage due to an earthquake event [9]. This curve assists in estimating various damage levels of the structure and for any type of structure. Incremental dynamic analysis (IDA) is a significant seismic engineering method for measuring fragility curves for a wide range of structures. This method was created to estimate the seismic risk for the structure encounters using the results of probabilistic seismic hazard analysis [10]. The analysis using IDA technique has been employed by Qu and Pan [11] and Farzampour et al. [12] in their studies to analyze the structure of seismic performance. Robinson et al. [13] demonstrated the structural fragility curves for several building categories. The result showed that the stone and mud building has 98% risk of collapse at 0.4 g. Moreover, based on the magnitude of 7.3 to 8.8 Mw, a Gorkha earthquake in 2015 caused several fatalities. The curves show that the earthquake, which had a magnitude of 7.3 Mw resulted in up to 100 000 fatalities. Collapse fragility curves indicate how the probability of structural damage increases as peak ground acceleration increases. In addition to the building material, the height of the structure affects the probability of damage.

In cases of low-rise RC buildings for fragility analysis measurement has been described by Adhikari et al. [14] by described comparative seismic vulnerability for several study conditions. The authors developed fragility analysis for slight, moderate, extensive, and complete damage for four cases: infill model without soil-structure interaction, bare frame model without soil-structure, infill model with soil structure, and bare frame model with soil-structure. As a result, when infills are predicted. The fundamental vibration time is greatly decreased. Fragility analysis generated for four instances shows that soil-structure interaction has a greater impact on lower damage states, whereas infills have a greater impact on higher damage states, increasing their exceedance probability at specific spectral acceleration levels.

The preparations against the seismic event in the seismic-prone area were not given enough consideration which led to the design of non-seismic structure not take seriously. An early earthquake warning (EEW) systems are designed to gives out a ground-shaking signal, allowing individuals and automated system to take preventive measures. This system has challenges in providing accurate and timely EEW signals for mid and high-rise buildings because to the potential differences in shaking experienced at different levels [15]. Deep learning, an instance of artificial intelligence (AI) that employs deep neural networks consisting of several layers, has shown considerable potential in improving the precision and efficiency of AI systems. Intelligent of EEW by deployments of deep learning has proposed by Saad et al. [16] by relies on a convolutional neural network to extract crucial features from waveforms, allowing the classifier to achieve strong performance in predicting earthquake parameters. The proposed technique has 93.67% and 89.50% classification accuracy for magnitude and location, respectively. Other studies that implemented deep learning in EEW were also proposed by Carratú et al. [17], Wibowo et al. [18] and Murshed et al. [19]. However, predicting the time and location of the subsequent seismic event is challenging. Despite earthquake predictions, community remains unsafe [15].

Therefore, to address limitations and failures of the structure due to earthquakes, it is necessary to regulate building structural behavior to assure safety and a more efficient design to prevent the structure from collapsing. The effectiveness with which structural vibration mitigation that applied directly to the building structure that may remove vibrations

has also attracted attention. Currently, a variety of control devices are being developed to guarantee the safety of the structure even though earthquakes cause high vibration amplitudes. A hybrid mass damper (HMD) is a control device that integrates an active control device with a tuned mass damper (TMD) and is cost-effective by decreasing the amount of energy needed to operate the system [20]. The installation of the HMD influences the building's performance in terms of minimizing seismic vibration. The top floor of the building is the optimum placement for HMD deployment [21]. Hybrid control has employed by Djedoui et al. [22] in their study for structural system using a base isolator, TMD and HMD. Based isolators are constructed between the foundation and the superstructure. The basic concept behind base isolation is that the response of the building structure is controlled so that the ground under the system can move while transferring little or no motion to the structure above. The type of excitation determines the efficiency of the base isolator. Considerable earthquakes can cause the base isolator reach critical conditions, resulting in large displacement, superstructure flexibility, isolation period and story number, can have a negative impact on the reliability of base isolation structures.

A control signal is generated by a control algorithm measured by the structural response to reduce the building vibration. The actuator will provide a secondary vibration response based on the control signal and minimize the overall building vibration. Chesné and Colette [23] deployed a simple control law technique to boost the efficiency and stability of a HMD consisting of one DOF system. Consequently, the presented HMD is both fail-safe and unconditionally stable in theory. Experimental work demonstrated the HMD's performance and robustness of the proposed technique. In [24], a robust adaptive controller is established to be utilized in the HMD system. The control approach is constructed to attenuate undesirable vibrations caused by an earthquake on multistory structures. A Lyapunov-based stability analysis strengthens the developed control design, demonstrating that the controller can maintain overall system stability while fulfilling the main control goal. It is proved that the proposed control method can be employed to meet the main control aim efficiently.

Nonsingular TSMC demonstrated superior character in in term of fast dynamic response, finite-time convergence, and high control accuracy [25]. This type of control strategy able to eliminate the paranormal phenomenon in the system's control input. When compared to traditional SMC, the nonsingular TSMC approach is better in reducing chattering [26]. The applications in spacecraft [27], vehicles [28], rigid manipulators [29], mechanical system [30], and autonomous underwater vehicle [31] have utilized nonsingular TSMC to address singularity obstacles with TSMC. It is crucial to choose an appropriate control strategy to give a signal to the actuator. With the current development of AI, the integrating of implementing neural network with the control strategy has been focus currently. Wang and Fei [32] enhanced nonsingular TSMC by integrating recurrent neural network (RNN) to more precisely estimate the unidentified element in a system compared to a traditional neural network due to the presence of feedback loops in its hidden layer, which retain weights and output signal as the feedback signals. The proposed controller validates that the compensation current effectively tracks the reference current in real-time. The proposed approached outperformed the SMC with the regular neural network in terms of tracking performance and durability. Integrating the neural network technique with nonsingular TSMC improves the resilience of the system control, particularly long short-term memory (LSTM). LSTM was first proposed by Hochreiter and Schmidhuber [33] in 1997. It is a variation of a RNN and is capable of selectively remembering patterns over long periods. RNN is a sophisticated deep learning method with a limited memory capacity that enables it to consider former network values in order to impact the current decision-making process according to the present input sequence. It is a great option for analyzing sequential data and is often used to understand the complexity [34]. The task of LSTM is utilized to estimate the variables in nonsingular TSMC. The study by Zhou et al. [35] employed LSTM in the prediction of high and low-complexity heating load features for building energy consumption.

The study has combined LSTM with other models and generated higher accuracy than a single deep learning model. Moreover, the performance of root mean square error (RMSE) and the average coefficient of determination was improved. Mohandes et al. [36] have discovered a growing interest in the application of newly developed artificial neural networks, such as RNN to building energy analysis areas due to its ability to improve the prediction of building energy analysis. Chang et al. [37] forecast the aggregated charging power demand for the electric vehicle using LSTM. The results from the study showed the forecasting outcomes using the proposed LSTM outperformed the other deep learning models by achieving good accuracy. In addition, LSTM is used to forecast an electrical short-term load as proposed by Ijaz et al. [38] by integrated along standard artificial neural network. Consequently, LSTM showed an excellent characteristic in forecasting the stochastic nature of an hour forward of electrical loads.

The control strategies of integrated nonsingular TSMC, nonsingular TSMC, and TSMC from previous studies are typically applied in vehicles, spacecraft, and robotic systems. However, there has been no empirical evidence on the impact of control strategies on mitigating the risk of building damage. On the other side, the proposed control strategy provides excellent vibration control capabilities. With the enhancement reported by [39], this work emphasizes the impact of control strategies, namely, integrated nonsingular TSMC, nonsingular TSMC, and TSMC, on preventing structural damage. Each proposed control strategy demonstrates its effectiveness in mitigating the probability of structural

damage and collapse by reducing vibration during an earthquake. Integrated nonsingular TSMC incorporates a neural network technique that can identify an acceptable value in the control strategy to fit the unknown value. All the proposed control strategies present a good response in terms of their ability to reduce vibration. Methodologies for assessing seismic vulnerability are frequently used to determine and control the risks of damage to buildings that are mostly related to the material and height of the structure [40]. This study highlights the employment of control strategies in mitigating the vibration using the fragility analysis for low-rise and high-rise buildings that are represented by mass, spring, and damper of 2-DOF and 10-DOF. In addition, the 2-DOF structure is validated using an experimental setup linked to LMS Test.Lab software. Previous studies performed various tests on many shaking tables such as in [41], and [42], but only a few have shaking tests connected to this software. As a result, this study demonstrated the details of experimental work constructed and linked to the LMS Test.Lab software. The experimental work response has strengthened the building structure that was developed in simulations. Overall, this study has significantly contributed based on;

a) The integration of deep learning techniques within the integrated nonsingular TSMC is a notable aspect of the research. This technique allows for the identification of acceptable values within the control strategies, thereby enhancing the adaptability to unknown variables and enhancing the performance.
b) The proposed control strategy highlights the excellent vibration control capabilities. This study emphasizes how the control strategy can effectively reduce vibration levels, hence, preventing structural damage and collapse during earthquakes.
c) The study focuses on applying these control strategies to low-rise and high-rise buildings, represented by 2-DOF and 10-DOF. Both systems showcase the versatility and practical implications of the research. The fragility analysis conducted provides insights into the effectiveness of these strategies in reducing structural vulnerability.
d) The study validated the 2-DOF structure through an experimental setup linked to the LMS Test.Lab software, has strengthened the credibility of the research findings.

Further, section II introduces the system design that consists of building structure and experimental work. Section III describes the control strategies proposed for the study that focus on integrated nonsingular TSMC, nonsingular TSMC, and TSMC. Apart from this, the performance of the control strategies proposed in the low-rise and high-rise buildings with the results have been mentioned in Section IV. Lastly, the conclusion has been discussed in Section V.

II. SYSTEM DESIGN

A. BUILDING STRUCTURE

The mass, spring, and damper, which comprise 2-DOF and 10-DOF, represent the building structures for low-rise and high-rise buildings. The controlling device, HMD is located on the building's top story. Figure 1 shows the system's building diagram for both building structures. Both building structures are illustrated in free-body diagrams to systematically analyze each floor of the structure are shown in Figure 2. The building structure represented by mathematical models is indicated in (1), (2), and (3), where m_1 and m_2 signify the mass of each level, the stiffness values are k_1, k_{n-1} and k_n, and the damping coefficients are c_1, c_{n-1} and c_n. For HMD, m_d, c_d and k_d are mass, damping, and stiffness coefficients. x_1, x_{n-1} and x_n are the displacement responses for each floor and control device. The acceleration of the ground motion is given by $\ddot{x}_g$.

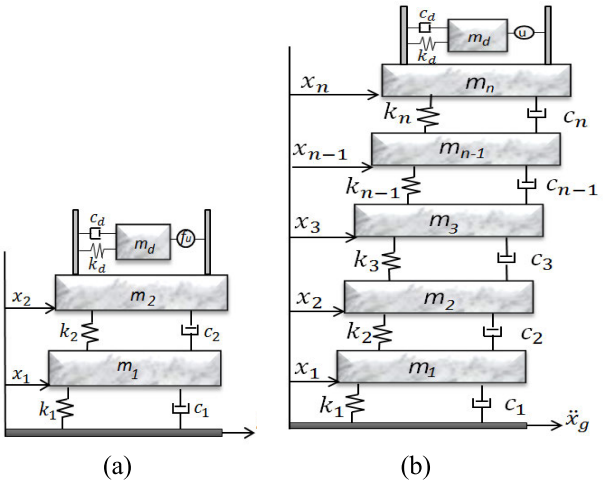

FIGURE 1. Schematic representation of the building for (a) 2-DOF and (b) 10-DOF system.

$$m_1\ddot{x}_1 + c_1\dot{x}_1 + k_1x_1 - c_n(\dot{x}_n - \dot{x}_1) - k_n(x_n - x_1) = -m_1\ddot{x}_g \tag{1}$$

$$m_n\ddot{x}_n + c_n(\dot{x}_n - \dot{x}_{n-1}) + k_n(x_n - x_{n-1}) - c_d(\dot{x}_d - \dot{x}_n) - k_d(x_d - x_n) = -m_n\ddot{x}_g - F_u \tag{2}$$

$$m\ddot{x}_d + c_d\dot{x}_d + k_dx_d - c_d\dot{x}_n - k_dx_n = -m_d\ddot{x}_g + F_u \tag{3}$$

The actuator controlled HMD, which is written as;

$$Ri + K_e(\dot{x}_d - \dot{x}_n) = u \tag{4}$$

$$F_u = K_f i \tag{5}$$

$$F_u = K_f\left[\frac{u - K_e[\dot{x}_d - \dot{x}_2]}{R}\right] \tag{6}$$

where u is the control voltage, K_f is the thrust constant, K_e is the induced voltage constant, R is the resistance value, F_u is the actuator's control force and i is current.

B. EXPERIMENTAL WORK

Figure 3 depicts the experimental work, which includes a mobile signal conditioning and data acquisition system (SCADAS), amplifier, shaker, accelerometer, and 2-DOF system. In this scenario, the shaker's vibration is arranged horizontally to replicate a similar seismic activity. The power

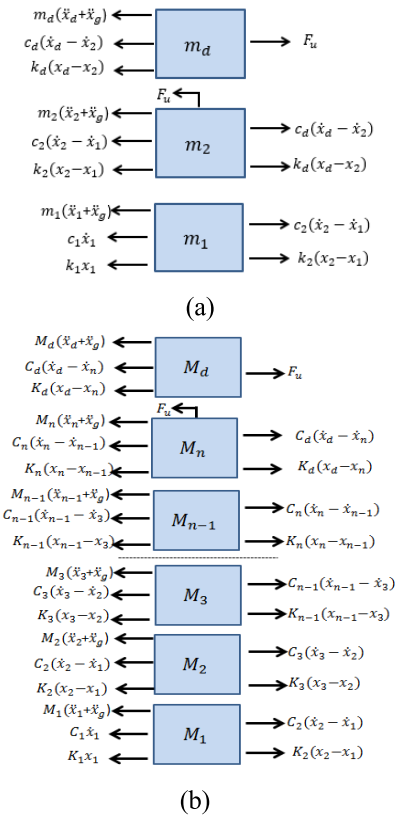

FIGURE 2. Free body diagram (a) 2-DOF and (b) 10-DOF structure.

amplifier received the signal from the input, which was then transmitted to the shaker. The required voltage or current of the amplifier is decided by the size of the system under test and the desired vibration levels. The accelerometer is used to detect and record the movement of the base and the mass of each floor. SCADAS is a modular data acquisition system comprised of a frame that stores all of the cards, as well as a power supply and controller. The power supply includes a battery for self-contained operation, with a capacity of up 2.5 hours. The mobile controller card is an ethernet interface with two encoder inputs and two output sources that are linked to the Test.Lab software. SCADAS is employed to measure dynamic signals, record accelerometer data, and connect to the Test.Lab software. The shaker was controlled by SCADAS and the data from this experiment was collected using LMS Test.Lab software. This software is intended for use in vibration testing of equipment. It also offers a robust built-in safety feature that decreases the chance of damaged items, as well as powerful analysis, simple reporting, and quick visualization. It provides accurate closed-loop control and has a strong built-in safety mechanism that reduces the possibility of damaged objects.

The connection between these components in experimental work is depicted in Figure 4. SCADAS memorizes the input excitation generated by the software for moving the shaker. The controller will send the signal to the amplifier, which will provide a vibration signal to the shaker. Each floor is equipped with accelerometers to measure the acceleration of the system and once the accelerometer detects the movement, the signal in acceleration value is delivered to SCADAS DAC. The response is then will be recorded by LMS Test.Lab software [43].

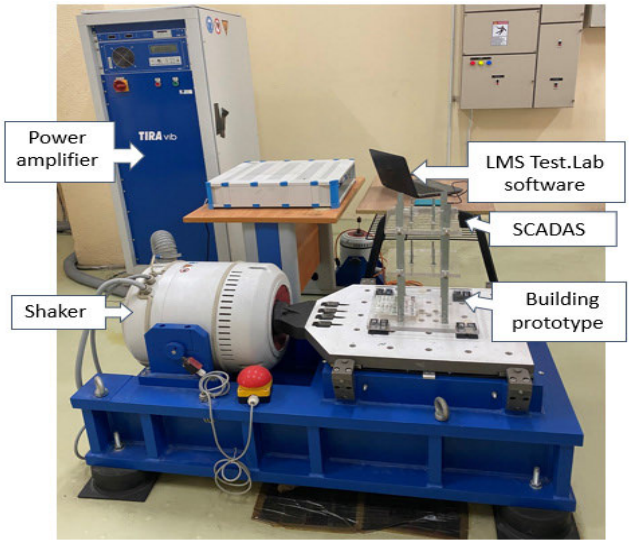

FIGURE 3. Experimental work setup.

TABLE 1. The parameter for experimental work.

Parameter	Unit	Value
Mass for each floor	Kg	0.764
Stiffness for each floor	N/m	182.9
Damping coefficient for each floor	N.s/m	30
Accelerometer sensitivity	mV/G	10
Shaker frequency range	Hz	2-4000
Amplifier output power	VA	4200
Signal-to-noise ratio	dB	> 80
Field current	A	6
Field voltage	V	100

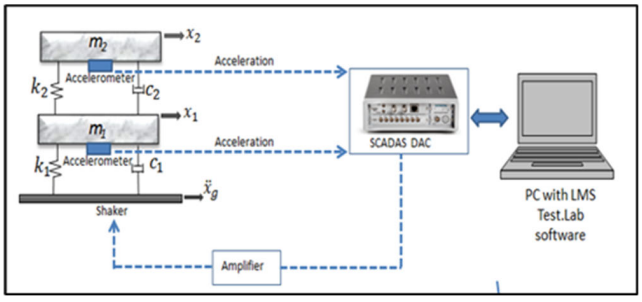

FIGURE 4. The connection for each component in experimental work.

Before experimenting, the closed-loop system is pretesting by specifying the SelfCheck parameter. SelfCheck configuration is utilized to examine the experiment setup

for faults with the connection, shaker, and amplifier. The program window status will generate a warning if there are any problems. Moreover, "Open Channel" was displayed if these cases occurred. This is due to the unstable connection between the accelerometer and the output of the data-gathering card. The accelerometer channel did not give a significant result above the background noise level. Additional errors that appeared during the SelfCheck setting were caused by DAC difficulties. The shaker amplifier's failure to deliver adequate output to run the full-scale equipment causes the DAC difficulty.

III. CONTROL STRATEGIES

Consider the building structure as;

$$\begin{cases} \dot{x}_1 = x_2 \\ \dot{x}_2 = f(x) + g(x)u + d(x) \end{cases} \tag{7}$$

where $x = [x_1, \ldots x_n, x_d]^T$, $f(x)$ and $g(x) \neq 0$ are nonlinear functions of x, $d(x)$ is uncertainty and disturbance and u is the scalar control input.

A. TERMINAL SLIDING MODE

The terminal sliding surface is defined by (8), where β is a design constant that must be greater than zero and the variables of p and q are positive odd integers that satisfy the condition of $p > q$.

$$s = x_n + \beta x_1^{\frac{q}{p}} \tag{8}$$

$$u = -g^{-1}(x)[f(x) + \beta \frac{q}{p} x_1^{\frac{q}{p}-1} x_n + \left(l_g + \eta\right) sgn(s)] \tag{9}$$

where $\eta > 0$

The stability analysis for TSMC is derived as follows:

$$\dot{s} = \dot{x}_n + \beta \frac{q}{p} x_1^{\frac{q}{p}-1} \dot{x}_1 \tag{10}$$

$$\dot{s} = f(x) + g(x)u + d(x) + \beta \frac{q}{p} x_1^{\frac{q}{p}-1} \dot{x}_1 \tag{11}$$

The equation in (9) is substituted into (11) to obtain;

$$\dot{s} = d(x) - \left(l_g + \eta\right) sgn(s) \tag{12}$$

$$s\dot{s} = sd(x) - \left(l_g + \eta\right)|s| \leq -\eta|s| \tag{13}$$

The singularity occurs if the value for $x_2 \neq 0$ when $s = 0$, according to the equation stated in (13). The problem appears during the reaching phase when the state approaches $s = 0$. Nonsingular TSMC is used to tackle this problem.

The following equation is used to develop a finite-time analysis for the system;

$$\int_{s=s(0)}^{s=s(t_r)} ds = \int_0^{tr} \pm n dt \tag{14}$$

$$s(t_r) - s(0) = \pm n t_r \tag{15}$$

$$t_r = s(0)/n \tag{16}$$

Suppose that after t_r, the attaining time which is the time of switching trajectory reach at the sliding surface, t_s from $x_1(t_r) \neq 0$ to $x_1(t_r + t_s) = 0$. In this phase $s = 0$,

$$x_2 + \beta x_1^{\frac{q}{p}} = 0 \tag{17}$$

$$\dot{x}_1 = -\beta x_1^{\frac{q}{p}} \tag{18}$$

The equation in (18) is integrated to obtain the equation (19) written as;

$$\int_{x_1(t_r)}^{0} x_1^{\frac{q}{p}} dx_1 = \int_{t_r}^{t_r+t_s} -\beta dt \tag{19}$$

$$-\frac{p}{p-q} x_1^{1-\frac{q}{p}}(t_r) = -\beta t_s \tag{20}$$

$$t_s = \frac{p}{\beta(p-q)} |x_1(t_r)|^{1-\frac{q}{p}} \tag{21}$$

B. NONSINGULAR TERMINAL SLIDING MODE CONTROL

Nonsingular TSMC has the advantage of providing a fast dynamic response, finite-time convergence, good control accuracy and is capable to eliminate irregular phenomena in the system's control input. This is represented by the following equations;

$$s = x_1 + \frac{1}{\beta} x_n^{\frac{p}{q}} \tag{22}$$

$$u = -g^{-1}(x)\left[f(x) + \beta \frac{q}{p} x_n^{2-\frac{p}{q}} + \left(l_g + \eta\right) + sgn(s)\right] \tag{23}$$

where $\beta > 0, p$ and q are both positive odd numbers, $1 < p/q < 2$, η is greater than zero and l_g is estimated using the adaptive law.

Analysis of the stability for nonsingular TSMC is written as;

$$\dot{s} = \dot{x}_1 + \frac{1}{\beta} \frac{p}{q} x_n^{\frac{p}{q}-1} \dot{x}_2 \tag{24}$$

$$\dot{s} = x_n + \frac{1}{\beta} \frac{p}{q} x_2^{\frac{p}{q}-1} (f(x) + g(x)u + d(x)) \tag{25}$$

Then, the equation (23) is substituted into (25) to obtain;

$$\dot{s} = \frac{1}{\beta} \frac{p}{q} x_2^{\frac{p}{q}-1} (d(x) - (l_g + \eta) \tag{26}$$

$$s\dot{s} = \frac{1}{\beta} \frac{p}{q} x_2^{\frac{p}{q}-1} \left(sd(x) - \left(l_g + \eta\right)|s|\right) \tag{27}$$

$$s\dot{s} \leq -\frac{1}{\beta} \frac{p}{q} \eta x_n^{\frac{p}{q}-1} |s| \tag{28}$$

When $x_n \neq 0, x_n^{\frac{p}{q}-1} > 0$ as p and q are positive integers. Thus, the results in equation (29) can be concluded that the Lyapunov condition is satisfied in the case of $x_2 \neq 0$.

$$-\frac{1}{\beta} \frac{p}{q} \eta x_n^{\frac{p}{q}-1} > 0 \tag{29}$$

The condition when $x_2 = 0$ is investigated by substituting the equation of (20) into (30) written as;

$$\dot{x}_2 = g(x) - \beta \frac{q}{p} x_n^{2-\frac{p}{q}} - \left(l_q + \eta\right) sgn(s) \tag{30}$$

$$\dot{x}_2 = g(x) - \left(l_g + \eta\right) sgn(s) \tag{31}$$

Since $s > 0$, resulted $\dot{x}_n \leq -\eta$ and when $s < 0$, resulted $\dot{x}_n \geq -\eta$. Therefore, the switching line $s = 0$ can be reached in a finite time. The sliding mode of $s = 0$ can be achieved from anywhere with the condition of switching trajectories in finite time.

C. LONG SHORT-TERM MEMORY

LSTM has been proposed as a technique for recursive neural network time dependence problems. It is a great tool with a large memory for predicting long-time series. However, it is crucial to ensure the timeliness of the provided prediction model. This study needs to predict the value of the upper bound of the uncertain parameter, l_g, in integrated nonsingular TSMC. It is important to ensure the building can overcome any other disturbances that impact the system and increase its robustness system. Therefore, the deployment of LSTM assists in predicting the value based on the trained technique from the existing value. The framework of LSTM consists of input, forget, and output gates as illustrated in Figure 5.

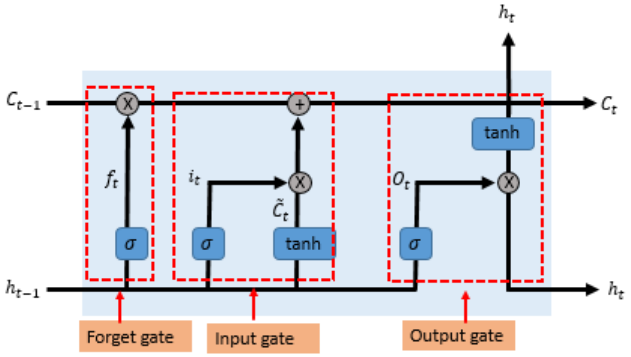

FIGURE 5. The structure of the LSTM model.

In the given formulas, i_t, O_t and f_t signify the state values of the input gate, output gate, and forget gate, respectively. The following are the LSTM calculation steps:

Step 1: LSTM can identify the information from the cell's old state, C_{t-1} to be eliminated by the forget gate based on the input, x_t and the state of the last hidden layer, h_{t-1}. The output of the current cell is as follows;

$$f_t = \sigma\left(w_f\left[h_{t-1}, x_t\right] + b_f\right) \tag{32}$$

where w_f is the weight matrix of the forget gate, b_f is the bias vector and σ is the activation function that typically uses the sigmoid function.

Step 2: The current input and the last output values are transferred to the input gate. The output i_t and candidate state $\tilde{C}_t$ are then written as;

$$i_t = \sigma(w_i[h_{t-1}, x_t] + b_i \tag{33}$$

$$\tilde{C}_t = \tanh\left(w_c.\left[h_{t-1}, x_t\right] + b_C\right) \tag{34}$$

Step 3: The state vector C_t is updated through the integration of the input of the forget gate with the last state of the cell described as;

$$C_t = f_t.C_{t-1} + i_t.\tilde{C}_t \tag{35}$$

Step 4: The output gate 0_t, is calculated using h_{t-1} and x_t. The output value of the LSTM neurons h_t is obtained from the output gate.

$$O_t = \sigma\left(W_o.\left[h_{t-1}, x_t\right] + b_o\right) \tag{36}$$

$$h_t = \sigma_t.\tanh\left(C_t\right) \tag{37}$$

where w_i, w_c and w_o are weight metrics of the input, cell, and output gate.

In this part, LSTM is employed to process the sequential trajectory data and generate a prediction value. LSTM network is trained and tested with the same dataset as the one used for displacement and velocity of nonsingular TSMC. During the training phase, several less important information are discarded to allow the memory cell to free up space for newer and more relevant information. The forget gate is intended to address this issue. The forget gate deletes or keeps information. The input gate is added to the LSTM structure if a value must be stored for many steps in the memory cell. And indeed the output gate is included to address the issue of multiple memories competing with each other. The LSTM neural network can be expressed once the memory gates are known.

Theorem 1: If the control law of integrated nonsingular terminal sliding mode control is designed as equation (23), the nonsingular TSMC manifolds given in equation (22) will reach equilibrium in finite time and tracking errors will converge in finite time. Alternatively, the building structure given in equation (7), might be considered.

Proof 1: The stability analysis of this controller conveys the Theorem 1 argument. Assume that $V = {}^1\!/_2 s^2$ is the candidate for the Lyapunov function. When this happens, the derivative of V along the trajectory is

$$\dot{V} = s\dot{s} \tag{38}$$

$$\dot{s} = \dot{x}_1 + \frac{1}{\beta}\frac{p}{q}x_2^{\frac{p}{q}-1}\dot{x}_2 \tag{39}$$

$$\dot{s} = x_2 + \frac{1}{\beta}\frac{p}{q}x_2^{\frac{q}{p}-1}\left[-\frac{k_T}{M}x_1 - \frac{c_T}{M} + \frac{1}{M}\left(u - f_d\right)\right] \tag{40}$$

The equation (42) is substituted into (45), resulting in equation (46) written as below;

$$\dot{s} = x_2 + \frac{1}{\beta}\frac{p}{q}x_2^{\frac{p}{q}-1}\left[-\frac{k_f}{M_T}x_1 - \frac{c_f}{M_T} + \frac{f_d}{M_T} + \frac{\left[k_f x_1 + c_f x_1 - M_T\beta\left(\frac{q}{p}\right)x_2^{2-\frac{p}{q}} - M_T\left(\xi + \eta\right)sgn\left(s\right)\right]}{M_T}\right] \tag{41}$$

$$\dot{s} = x_2 + \frac{1}{\beta}\frac{p}{q}x_2^{\frac{p}{q}-1}\left[-\frac{f_d}{M_T} - \beta\left(\frac{q}{p}\right)x_2^{2-\frac{p}{q}} - \left(\xi + \eta\right)sgn(s)\right. \tag{42}$$

$$\dot{s} = -\left(\xi + \eta\right)sgn\left(s\right) - \frac{f_d}{M} \tag{43}$$

The sliding surface estimation error is written as;

$$s_e = s - \hat{s} = \hat{x}_2 \tag{44}$$

This generates equation (50), where ξ is the adaptive law value.

$$\dot{V} = s\dot{s} = \left(s - \hat{s} + \hat{s}\right)\left(-\frac{f_d}{M} - (\xi + \eta)\, sgn\left(\hat{s}\right)\right) \tag{45}$$

$$\dot{V} = \left(s - \hat{x}_2\right)\left(-\frac{f_d}{M} - (\xi + \eta)\, \mathrm{sgn}\left(\hat{s}\right)\right) \tag{46}$$

The equation above is solved to get the equation as follows;

$$\dot{V} = -\frac{f_d}{M}s + \frac{f_d}{M}\hat{x}_2 - (\xi + \eta)\, sgn\left|\hat{s}\right| + \hat{x}_2\,(\xi + \eta)\, sgn\left(\hat{s}\right) \tag{47}$$

where $\frac{f_d}{M} \leq \xi$,

$$\dot{V} = \hat{s}\xi + \hat{x}_2 - (\xi + \eta)\, sgn\left|\hat{s}\right| + \hat{x}_2\,(\xi + \eta) \tag{48}$$

$$\dot{V}\,(t) = \dot{s}s =\leq -\eta\left|\hat{s}\right| \tag{49}$$

That is,

$$\dot{V} \leq -\eta\,|\mathrm{s}| < 0, \;\; \text{for s} \neq 0 \tag{50}$$

The nonsingular TSMC's Lyapunov controller stability for the building structure can be assessed using equation (50). The value of η is 0.01 and the sliding surface was calculated using the value of $|4\times10^{-8}|$, which gave the result of 0.04×10^{-8}. As a result, the value achieved is less than 0, demonstrating that the nonsingular TSMC manifold of the controller converges to zero in a finite time. Nevertheless, if (39) is attained, the output tracking error of the building structure will converge to zero in a finite time, demonstrating the system's stability and robustness. This concludes the Theorem 1 proof.

Figure 6 shows the block diagram of the implementation of integrated nonsingular TSMC with the building structure to mitigate the building vibration, where x_f is the target value for the system output, e is an error, s is the sliding surface, u is the control input and the output feedback is the building structure's displacement and velocity. The input excitation to the building is fed with the real earthquake data taken from Pondaguitan, Philippines with 7.0 *Mw*. LSTM is deployed to predict the upper bound of uncertain value, l_g for integrated nonsingular TSMC by using the dataset value generated by nonsingular TSMC. The test data and predict data consist of 16 000 variables for 2-DOF and 10 000 variables for the 10-DOF system. The simulation data construct with 100 epochs and obtained RMSE for 2-DOF and 10-DOF are 0.11 and 0.24, respectively. While increasing the number of training epochs can enhance accuracy to a certain extent, it is crucial to balance training to avoid overfitting. Techniques such as validation and regularization are essential to ensure that the model generalizes well to unseen data. In addition, the performance of the predicted upper bound of unknown parameters was evaluated using the mean absolute error (MAE) and mean squared error (MSE). The MAE for the 2-DOF and 10-DOF systems were calculated to have values of 0.081709 and 0.19022. The MSE values for the 2-DOF and 10-DOF systems are 0.013247 and 0.057421, respectively. Figure 7 is the predicted and actual result generated from the study. The proximity of these results shows the efficiency of LSTM based model. In addition, the results highlight the efficiency and robustness of the LSTM based model in predicting the upper bound of uncertain values for both 2-DOF and 10-DOF systems. The close match between actual and predicted values, as evidenced by the low RMSE has validates the capability of the model to generalize from the training data and accurately forecast outcomes. Similarly, the small MAE values demonstrate that the average magnitude of the prediction errors is minimal, indicating accurate and consistent performance. In addition, the small MSE values highlight the ability of the model to successfully manage significant errors, leading to a significant level of reliability. This comprehensive evaluation of RMSE, MAE, and MSE establishes the utility of the model in integrating control strategy and enhancing the durability of the building structure by ensuring robust and accurate predictions.

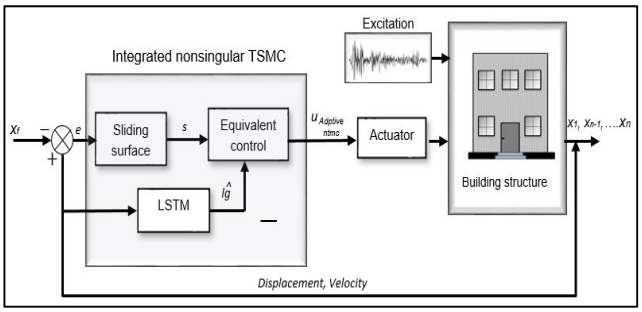

FIGURE 6. Block diagram of the control system.

IV. RESULT AND DISCUSSION

A. SYSTEM VALIDATION

The building structure model designed in Matlab is validated using the LMS Test.Lab software and an experimental setup. The input and output of the structural system used in this experiment are measured in acceleration values since accelerometers are used. Various inputs are supplied to validate the building structure model based on various seismic events. Figure 8 depicts the acceleration output measured from the experimental work. The accelerometer was used to measure the acceleration for base input, second floor and first floor with ranges of Figures 8 (a), (b) and (c). The value for base input acceleration serves as the reference point for evaluating the response of the other floors. The value for the first floor shows a significant reduction in acceleration compared to the base input, indicating that the building absorbs and dissipates the energy that is introduced by the ground motion. The further reduction measured on the second floor shows the cumulative effect of the structural damping. The performance of acceleration response at different floors validates the building structure by demonstrating the experimental results align with the theoretical predictions.

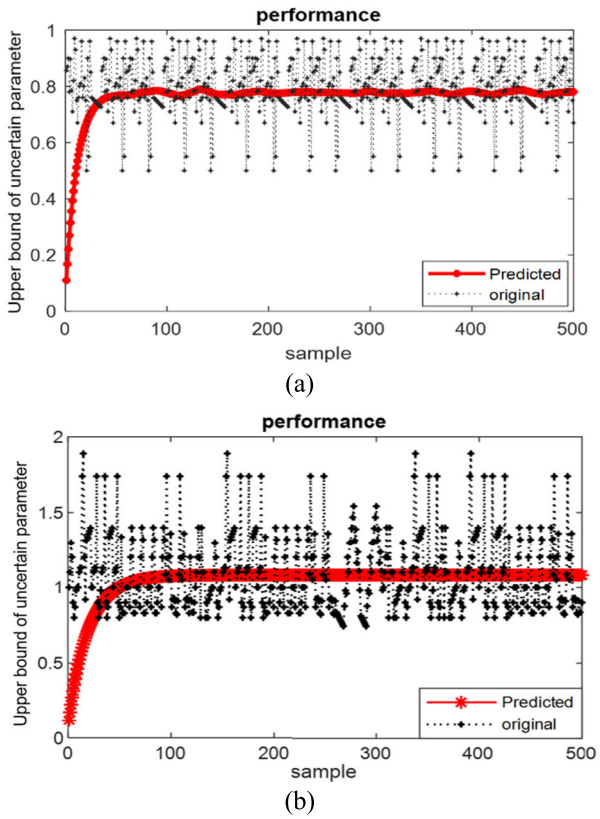

FIGURE 7. Plot between actual and predicted value (a) 2-DOF (b) 10-DOF system.

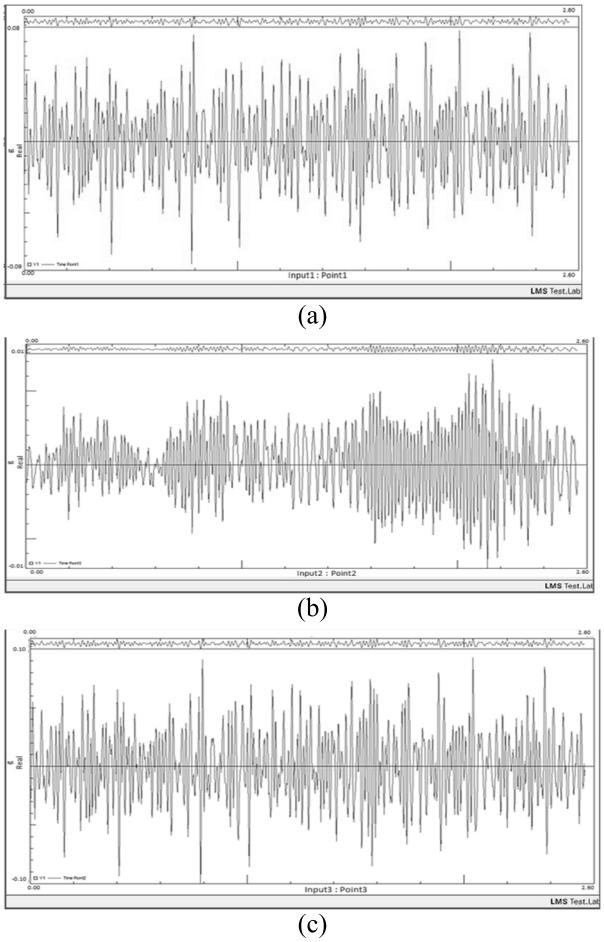

FIGURE 8. Acceleration performance obtained from experimental work (a) basement input (b) first floor (c) second floor.

The results of the experimental and simulation work are summarised in Figure 9. As depicted in the figures, the results of both approaches have quite similar minimum and maximum ranges. The acceleration ranges for ground input plots in Figure 9 (a) display identical performance between simulation and experimental data, showing the same inputs were given to the system. The same input values to both the simulation and the hardware are essential to validate the system by measuring the response of the first and second floor accelerations. This approach ensures comparability, accurate validation and ensuring that the simulation model can be trusted to realistically reflect the physical system's behavior under identical conditions. Based on this ground input, the results for the first floor and second floor were measured by using an accelerometer that was placed below the mass of the structure. The results for the first and second floors exhibited a slight difference, with experimental data showing marginally higher acceleration values compared to the simulation. The acceleration ranges for the first and second floors are 0.01 m/s^2 and 0.1 m/s^2, respectively. Experimental accelerations can be affected by a sensor placement that was measured by an accelerometer or external disturbances that might not be fully replicated in the simulation model. The close alignment in the minimum and maximum acceleration ranges observed in both the simulation and experimental data suggests that the model accurately captures the essential dynamics of the building structure. The high similarity in the ranges indicates that the simulation provides a reliable approximation of the real-world implementation and, thus, reinforces the validity of the structure. However, minor discrepancies between the simulation and experimental results might still be present, which are expected in such studies.

B. IMPLEMENTATION OF THE CONTROL STRATEGY

The building structure is installed with HMD in the numerical simulation, including the deployment of the control technique. The parameters in Table 2, which consist of mass, stiffness and damping are selected to represent typical characteristic of low-rise and high-rise buildings. These parameters are crucial in the numerical simulations as these parameters directly influence the dynamic response of the structure and the effectiveness of the control strategy. As depicted in Table 2, the actual parameter is used to assess the controller's effectiveness in actual life taken from [44]. The mass represents the inertia of the building floors, the stiffness refers to the structural rigidity and the dampring depicted the energy dissipation capacity. Utilizing these parameters able to accurately simulate the building behaviour under various loads and therefore measure the performance of the control strategy mitigates the vibrations and enhance structural durability. The input excitation is provided as a disturbance

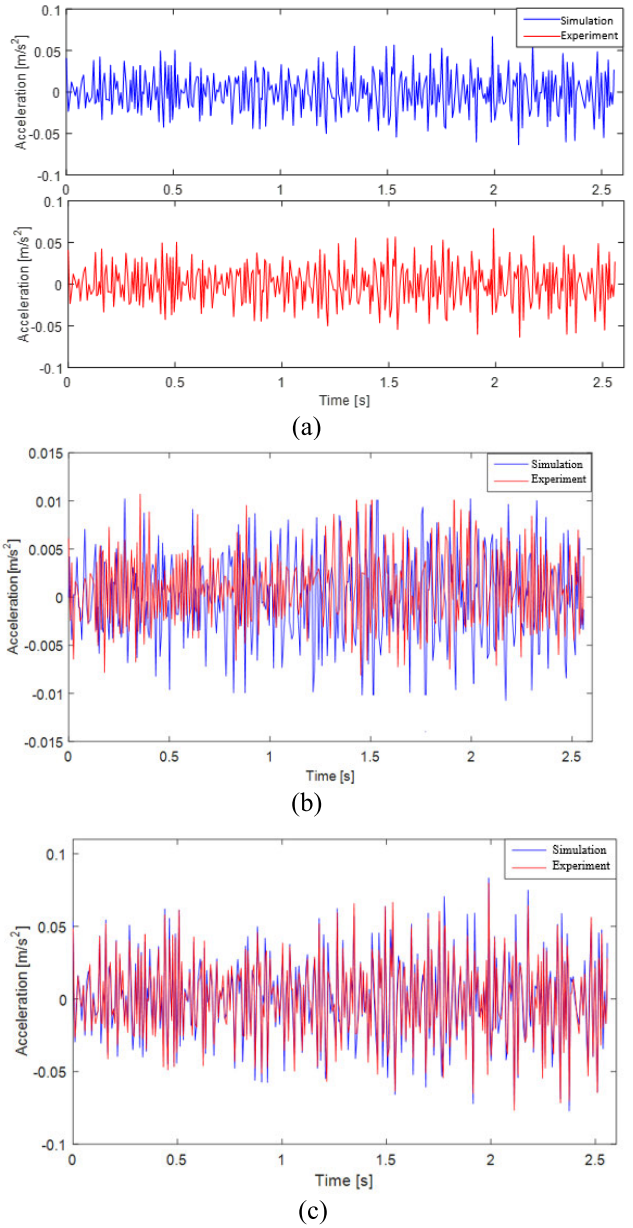

FIGURE 9. Comparison of the plots from the simulation and experimental work (a) ground input (b) first floor output response (c) second floor output response.

to evaluate the control strategy's robustness, based on the real earthquakes that happened in Pondaguitan, Philippines occured on January 21, 2021, with a magnitude of 7.0 Mw.

1) LOW-RISE BUILDING

The impact of control strategy implementation for a low-rise building that represent by 2-DOF System is simulated using Simulink/Matlab to study the effectiveness in mitigation of earthquake events. Figure 10 shows the findings for the building structure for the second and first floors, respectively. The result indicated that earthquake-induced vibrations were successfully controlled after control techniques were implemented. The maximum vibration that occurred on the second floor is at 46 s, resulting in a 43% reduction percentage for integrated nonsingular tSM, 36% for nonsingular TSMC, and 23% for TSMC recorded in contrast to the uncontrolled system. The first floor causes a 40% decrease for integrated nonsingular TSMC, 38% reduction for nonsingular TSMC, and 7.5% reduction for TSMC. In comparison to the other controllers, the integrated nonsingular TSMC has superior performance in terms of reducing the vibration of the building.

TABLE 2. System parameter.

Number of floors		Mass ($10e^3$kg)	Stiffness ($10e^5$N/m)	Damping ($10e^5$N.s/m)
Low-rise building	First and second floor	320	930	15.69
High-rise building	First until tenth floor	320	930	15.69
HMD		44	36.7	0.71

The findings clearly indicate that the integrated nonsingular TSMC exhibits superior performance in both the second and first floors, highlighting its effectiveness in controlling earthquake-induced vibrations. The enhanced reduction percentages suggest that this control strategy offers better robustness and adaptability to dynamic changes compared to the nonsingular TSMC and TSMC. The nonsingular TSMC also shows strong performance, significantly reducing displacements but slightly lagging behind the integrated approach. This indicates its robustness but also points to potential areas for improvement in handling nonlinear dynamics and interaction effects more effectively. The TSMC, while effective in reducing vibrations, shows the least performance among the strategies tested. Its lower reduction percentages reflect its limitations in addressing more complex dynamics introduced by seismic events.

Figure 11 shows the sliding surface for each controller. Once the sliding mode has been established, the sliding surface design must therefore correspond to the appropriate specifications. As demonstrated by the figures, the state trajectories are moving towards the sliding surface, which was set to 0 to keep the system stable during an earthquake. This provided the system with the necessary reaction to obtain a stable condition.

According to the performance of the implementation of control strategies in building systems, three measurement metrics have been calculated to assess the displacement response, which is RMSE, MAE, and MSE. This evaluation is crucial for understanding the effectiveness of the controllers in mitigating vibrations caused by earthquakes. The results for these measurement metrics are shown in Table 3. For the low-rise building, the integrated nonsingular TSMC

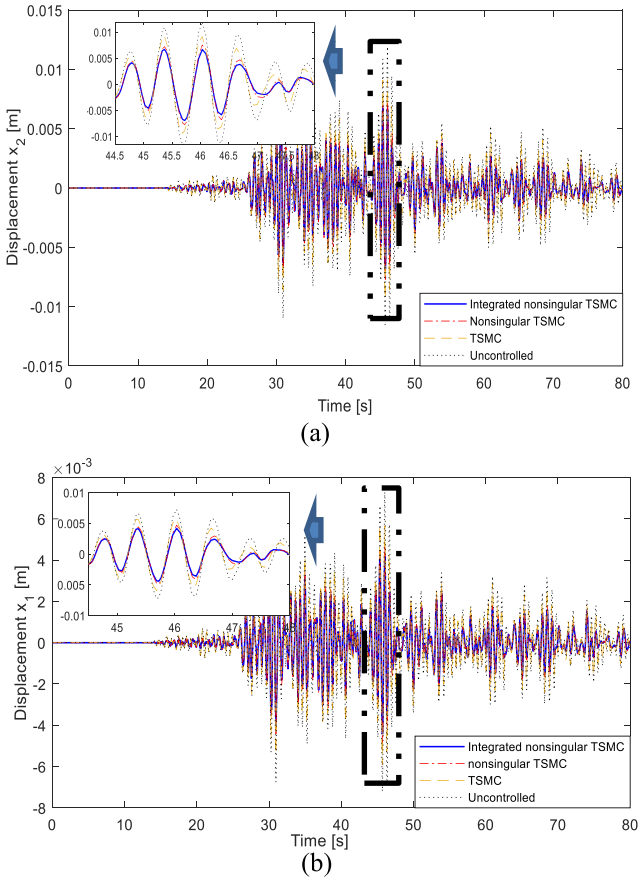

FIGURE 10. The comparison of control strategy implementation for the displacement response measured at (a) second floor (b) first floor.

demonstrates the most superior control among the three controllers, as indicated by its lowest RMSE and MAE values. This demonstrates that the deployment of LSTM allows it to predict and adapt to parameter uncertainties effectively and thus, results in superior vibration suppression. The nonsingular TSMC also performs well, though not as finely tuned as the integrated deep learning approach. TSMC shows the highest error metrics indicating less effective control compared to its counterparts. In high-rise buildings, the integrated nonsingular TSMC again shows the best performance. The RMSE and MAE values are the lowest, highlighting its capability to adapt and predict parameter changes effectively, which is crucial for managing the dynamics of a taller structure. The nonsingular TSMC outperforms the TSMC, indicating that eliminating singularities while optimizing control response could enhance building vibration suppression. TSMC is still effective in suppressing the vibration. However, the controller is less optimal for high-rise buildings, as reflected in its higher error metrics.

Figure 12 summarises the results that were measured on the first and second floors during the building structure's maximum vibration, which occurred at 46 s. According to both figures, the second story swayed more than the first floor during the seismic activity. On the other hand, the vibrations were reduced when control strategies were implemented.

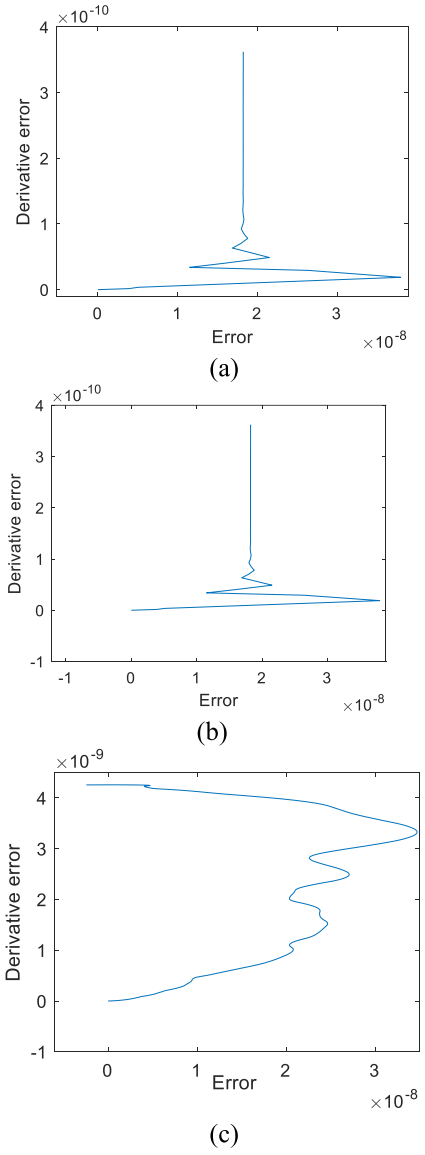

FIGURE 11. Sliding surface (a) Integrated nonsingular TSMC (b) Nonsingular TSMC (c) TSMC.

This study takes into consideration ductile RC buildings and the probability of a structure collapsing is approximated using the graph of probability damage for low-rise buildings under the 3-DOF system, utilizing the code C1L as specified by FEMA [6] and structural response under seismic load is evaluated using Incremental Dynamic Analysis (IDA) [45]. According to the probability of collapse, it is evident that using the proposed controller, integrated nonsingular TSMC in the 2-DOF structure has decreased the percentage of the building from collapse. Figure 13 shows that the probability of the building having slight damage is 100%, but after the integrated nonsingular TSMC is implemented, the probability decreases to 12%. Moreover, the probability percentage of the building suffering moderate damage is reduced from 92% to 5%, extensive damage from 55% to 3%, and complete damage from 18% to 1%. The implementation of the controller in the building structure shows the response demonstrates

TABLE 3. Performance evaluation metrics.

Controllers	RMSE	MAE	MSE
Low-rise building			
Integrated nonsingular TSMC	8.807 × 10^{-8}	7.757 × 10^{-15}	6.268 × 10^{-8}
Nonsingular TSMC	4.422 × 10^{-7}	1.955 × 10^{-13}	6.268 × 10^{-8}
TSMC	2.815 × 10^{-6}	7.921 × 10^{-12}	6.268 × 10^{-8}
High-rise building			
Integrated nonsingular TSMC	6.052 x 10^{-4}	3.663 × 10^{-7}	6.847 × 10^{-5}
Nonsingular TSMC	6.783 x 10^{-4}	4.601 × 10^{-7}	6.847 × 10^{-5}
TSMC	5.260 x 10^{-3}	2.768 × 10^{-5}	6.847 × 10^{-5}

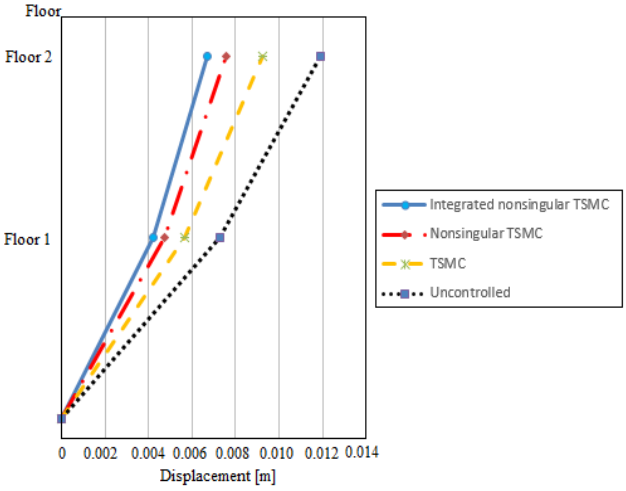

FIGURE 12. The response of the building to the implementation of the control strategy.

impressive benefits in minimizing the probability of the building collapse.

2) HIGH-RISE BUILDING

The efficiency of the control strategy is then deployed by improving the building structure for 10-DOF that demonstrate high-rise buildings. Figure 14 illustrates the results obtained for displacement performance evaluated on the tenth, fifth, and first floors. For the tenth floor, the maximum vibration occurred at 54.5 s. According to the total reduction compared to the uncontrolled structure, integrated nonsingular TSMC reduction is up to 83%, while nonsingular TSMC is down to 79% and TSMC is down to 4.34% recorded for the tenth floor. Based on the first floor, the percentage of vibration suppression recorded from the uncontrolled structure for each controller approach is 75% for integrated nonsingular TSMC, 68% for nonsingular TSMC, and 0.16% for TSMC. These results indicate that using LSTM in nonsingular TSMC

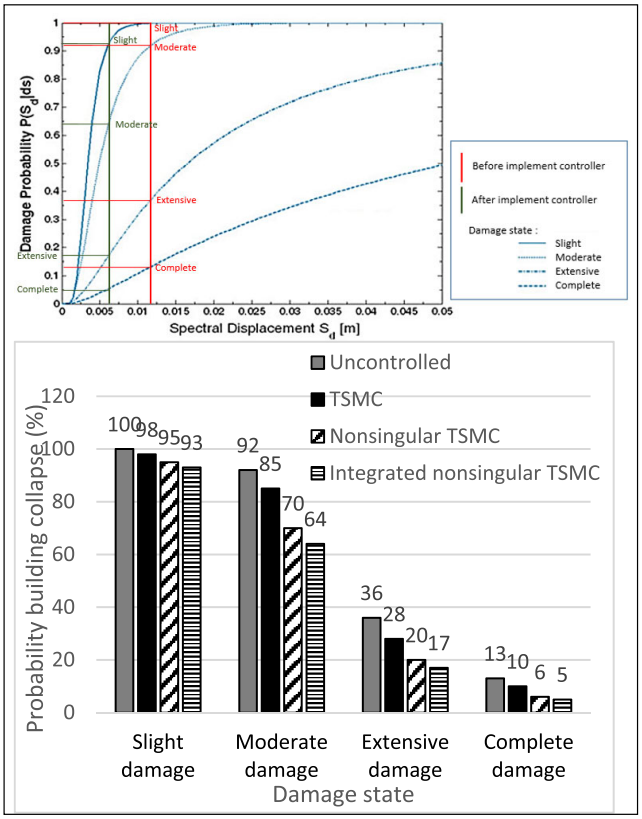

FIGURE 13. Probability of the low-rise building collapse.

assists predict the controller with a better response. Additionally, this integrated controller has a better response in suppressing building vibration. The rest of the displacement performance measured on another floor generated all the control strategies utilized in this study have successfully decreased the vibration of the building. However, compared to each other, integrated nonsingular TSMC has a better response with respect to vibration reduction.

Figure 15 shows the displacement response for each storey and each controller for this high-rise building. The tabulated data for high-rise buildings is taken at the maximum vibration that occurred to the system. The curve result shows the highest floor is risky as it generates higher sway compared to the below floor. Consequently, once a large vibration impacts a structure, structural damage including wall cracking and severe floor slope can be noticed. Therefore, to avoid this drawback the control strategy that is implemented in the structure can prevent this from occurring. All the control strategies deployed in this study have decreased the vibration however compared to the others, an integrated nonsingular TSMC has superior performance in suppressing the vibration.

The building collapse probability for reinforced concrete high-rise buildings is using the code of C1H as prescribed by FEMA and IDA. Figure 16 shows the probability of damage to the system. Based on the result, it is seen clearly that the implementation of the proposed controller has reduced the percentage of the building from collapse. The reduction of the probability for the building to have slight damage is

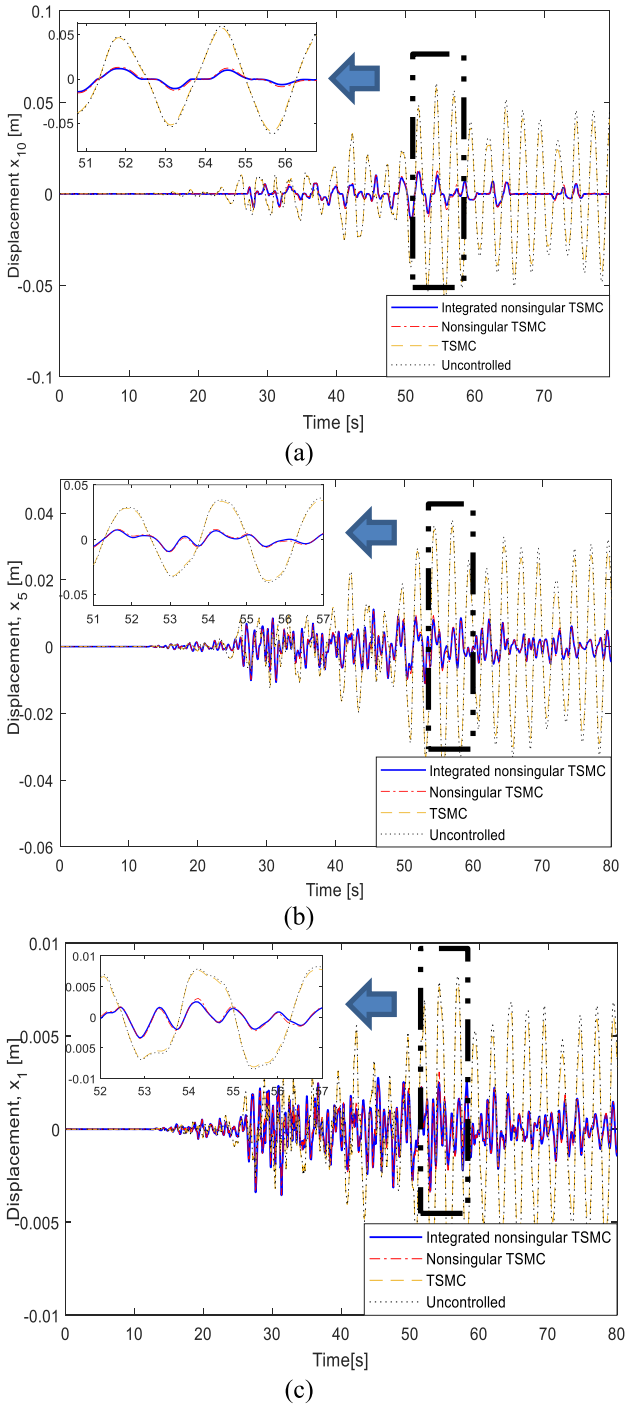

FIGURE 14. The comparison of control strategy implementation for the displacement response measured at (a) tenth floor (b) fifth floor (c) first floor.

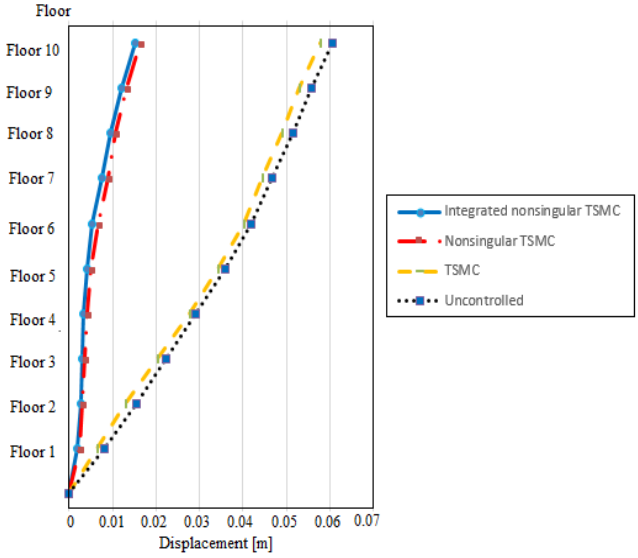

FIGURE 15. Displacement response for each floor.

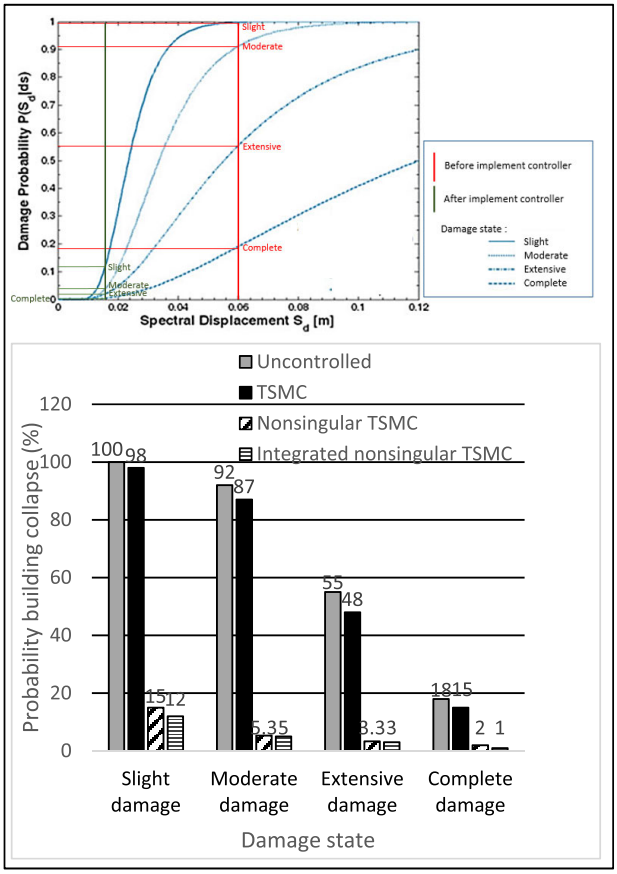

FIGURE 16. Probability damage for the high-rise building to collapse.

100% and reduce to 12% with the deployment of integrated nonsingular TSMC by moderate damage, the damage probability is reduced from 92% to 5%, extensive damage with 55% reduced to 3% and complete damage is reduced with 18% to 1%. There is not much different reduction percentage of integrated nonsingular and nonsingular TSMC due to the utilization of LSTM in that control strategy that predicts the value based on the actual value in nonsingular TSMC. However, this implementation assists the proposed controller in predicting the value to obtain a good performance.

V. CONCLUSION

The objective of this study was to investigate how adopting control strategies, such as integrated nonsingular TSMC, nonsingular TSMC, and TSMC, to a 2-DOF and 10-DOF

structure could improve the building's structural integrity while minimizing the probability of damage. Experimental work on the 2-DOF structure established the system and acceleration response was assessed using the LMS Test.Lab software. The simulation results using Matlab were compared with the outcome of the building system response. Integrated nonsingular TSMC using deep learning was created to improve structural performance by mitigating vibration during an earthquake event. The controller's efficiency was compared to those of TSMC and nonsingular TSMC. All the control strategies have reached equilibrium and maintain their position as the intended response specified, demonstrating the stability of the controller. In addition, all the control strategies suppress the building vibration and decrease the probability of structural damage to the building. The control strategies in this study have successfully mitigated the vibration due to earthquake events. The implementation of integrated nonsingular TSMC has resulted in the possibility of a building having minor damage decreasing to 43%, compared to an uncontrolled building which has a 100% chance of having slight damage. The smaller percentage of buildings that are prone to damage demonstrated the major influence of implementing a control strategy in the building structure.

REFERENCES

[1] H. Liu, C. Song, Z. Li, Z. Liu, L. Ta, X. Zhang, B. Chen, B. Han, and J. Peng, "A new method for the identification of earthquake-damaged buildings using Sentinel-1 multitemporal coherence optimized by homogeneous SAR pixels and histogram matching," *IEEE J. Sel. Topics Appl. Earth Observ. Remote Sens.*, vol. 17, pp. 7124–7143, 2024.

[2] S. Update. (2018). *Situation Update, no.15-Final 7.4 Earthquake and Tsunami. 2018*. Accessed: May 2, 2019. [Online]. Available: https://ahacentre.org/situation-update/

[3] G. Grunthal and R. M. W. Musson, "Earthquakes, intensity," *Encyclopedia Solid Earth Geophysics*, vol. 1, pp. 1–7, Jun. 2020.

[4] X. Duan and J. W. Pappin, "A procedure for establishing fragility functions for seismic loss estimate of existing buildings based on nonlinear pushover analysis," in *Proc. 14th World Conf. Earthquake Eng.*, 2008, pp. 1–24.

[5] E. Peyghaleh, V. Mahmoudabadi, J. R. Martin, A. Shahjouei, Q. Chen, M. Javanbarg, and S. Khoshnevisan, "Impact of local site conditions on portfolio earthquake loss estimation for different building types," *Natural Hazards*, vol. 94, no. 1, pp. 121–150, Oct. 2018.

[6] *HAZUS-MH MR4 Multi-Hazar D Loss Estimation Methodology—Earthquake Model: Technical Manual. Department of Homeland Security*, Federal Emergency Manage. Agency (FEMA), Washington, DC, USA, 2003.

[7] J. Alam, M. Hussan, and A. Sarraz, "Seismic fragility assessment of RC building using nonlinear static pushover analysis," in *Proc. Int. Conf. Planning, Archit. Civil Eng.*, 2017, vol. 26, no. 3, p. 7.

[8] L. Giresini, C. Casapulla, R. Denysiuk, J. Matos, and M. Sassu, "Fragility curves for free and restrained rocking masonry façades in one-sided motion," *Eng. Struct.*, vol. 164, pp. 195–213, Jun. 2018.

[9] X. Yuan, G. Chen, P. Jiao, L. Li, J. Han, and H. Zhang, "A neural network-based multivariate seismic classifier for simultaneous post-earthquake fragility estimation and damage classification," *Eng. Struct.*, vol. 255, Mar. 2022, Art. no. 113918.

[10] A. Gkimprixis, E. Tubaldi, and J. Douglas, "Evaluating alternative approaches for the seismic design of structures," *Bull. Earthq. Eng.*, vol. 18, no. 9, pp. 4331–4361, Jul. 2020.

[11] J. Qu and C. Pan, "Incremental dynamic analysis considering main aftershock of structures based on the correlation of maximum and residual inter-story drift ratios," *Appl. Sci.*, vol. 12, no. 4, p. 2042, Feb. 2022.

[12] A. Farzampour, I. Mansouri, and H. Dehghani, "Incremental dynamic analysis for estimating seismic performance of multi-story buildings with butterfly-shaped structural dampers," *Buildings*, vol. 9, no. 4, p. 78, Apr. 2019.

[13] T. R. Robinson, N. J. Rosser, A. L. Densmore, K. J. Oven, S. N. Shrestha, and R. Guragain, "Use of scenario ensembles for deriving seismic risk," *Proc. Nat. Acad. Sci. USA*, vol. 115, no. 41, pp. E9532–E9541, Oct. 2018, doi: 10.1073/PNAS.1807433115.

[14] R. Adhikari, R. Rupakhety, P. Giri, R. Baruwal, R. Subedi, R. Gautam, and D. Gautam, "Seismic fragility analysis of low-rise RC buildings with brick infills in high seismic region with alluvial deposits," *Buildings*, vol. 12, no. 1, p. 72, Jan. 2022.

[15] G. Cremen, O. Velazquez, B. Orihuela, and C. Galasso, "Predicting approximate seismic responses in multistory buildings from real-time earthquake source information, for earthquake early warning applications," *Bull. Earthq. Eng.*, vol. 19, no. 12, pp. 4865–4885, Sep. 2021.

[16] O. M. Saad, A. G. Hafez, and M. S. Soliman, "Deep learning approach for earthquake parameters classification in earthquake early warning system," *IEEE Geosci. Remote Sens. Lett.*, vol. 18, no. 7, pp. 1293–1297, Jul. 2021.

[17] M. Carrato, V. Gallo, V. Paciello, and A. Pietrosanto, "A deep learning approach for the development of an early earthquake warning system," in *Proc. IEEE Int. Instrum. Meas. Technol. Conf.*, May 2022, pp. 1–6.

[18] A. Wibowo, C. Pratama, D. P. Sahara, L. S. Heliani, S. Rasyid, Z. Akbar, F. Muttaqy, and A. Sudrajat, "Earthquake early warning system using ncheck and hard-shared orthogonal multitarget regression on deep learning," *IEEE Geosci. Remote Sens. Lett.*, vol. 19, pp. 1–5, 2022, doi: 10.1109/LGRS.2021.3066346.

[19] R. U. Murshed, K. Noshin, M. A. Zakaria, M. F. Uddin, A. F. M. S. Amin, and M. E. Ali, "Real-time seismic intensity prediction using self-supervised contrastive GNN for earthquake early warning," *IEEE Trans. Geosci. Remote Sens.*, vol. 62, 2024.

[20] S. Thenozhi and W. Yu, "Advances in modeling and vibration control of building structures," *Annu. Rev. Control*, vol. 37, no. 2, pp. 346–364, Dec. 2013.

[21] N. Mamat, F. Yakub, S. A. Z. S. Salim, M. S. M. Ali, and S. M. S. M. Putra, "Analysis of implementation control device in hybrid mass damper system," in *Proc. IEEE Int. Conf. Autom. Control Intell. Syst.*, Oct. 2018, pp. 123–127.

[22] N. Djedoui, A. Ounis, J. P. Pinelli, and M. Abdeddaim, "Hybrid control systems for rigid buildings structures under strong earthquakes," *Asian J. Civil Eng.*, vol. 18, no. 6, pp. 893–909, 2017.

[23] S. Chesné and C. Collette, "Experimental validation of fail-safe hybrid mass damper," *J. Vibrat. Control*, vol. 24, no. 19, pp. 4395–4406, Oct. 2018.

[24] R. C. Ümütlü, H. Ozturk, and B. Bidikli, "A robust adaptive control design for active tuned mass damper systems of multistory buildings," *J. Vibrat. Control*, vol. 27, nos. 23–24, pp. 2765–2777, Dec. 2021.

[25] A. R. Laware, S. K. Awaze, V. S. Bandal, and D. B. Talange, "Experimental validation of the non-singular terminal sliding mode controller for a process control system," *ECTI Trans. Electr. Eng., Electron., Commun.*, vol. 21, no. 1, Feb. 2023, Art. no. 248553.

[26] W. Xu, Y. Jiang, C. Mu, and H. Yue, "Nonsingular terminal sliding mode control for the speed regulation of permanent magnet synchronous motor with parameter uncertainties," in *Proc. 18th Int. Conf. Elect. Mach. Syst.*, 2015, pp. 1–26, doi: 10.1109/IECON.2015.7392393.

[27] S. Eshghi and R. Varatharajoo, "Nonsingular terminal sliding mode control technique for attitude tracking problem of a small satellite with combined energy and attitude control system (CEACS)," *Aerosp. Sci. Technol.*, vol. 76, pp. 14–26, May 2018.

[28] D. Ning, S. Sun, H. Du, W. Li, and W. Li, "Control of a multiple-DOF vehicle seat suspension with roll and vertical vibration," *J. Sound Vibrat.*, vol. 435, pp. 170–191, Nov. 2018, doi: 10.1016/J.JSV.2018.08.005.

[29] J. Zhai and G. Xu, "A novel non-singular terminal sliding mode trajectory tracking control for robotic manipulators," *IEEE Trans. Circuits Syst. II, Exp. Briefs*, vol. 68, no. 1, pp. 391–395, Jan. 2021.

[30] R. Rascón, D. I. Rosas, and J. C. Rodríguez-Quiñonez, "Robust continuous control for a class of mechanical systems based on nonsingular terminal sliding mode," *IEEE Access*, vol. 8, pp. 19297–19305, 2020, doi: 10.1109/ACCESS.2020.2965596.

[31] X. Yang, X. Zhu, W. Liu, H. Ye, W. Xue, C. Yan, and W. Xu, "A hybrid autonomous recovery scheme for AUV based Dubins path and non-singular terminal sliding mode control method," *IEEE Access*, vol. 10, pp. 61265–61276, 2022, doi: 10.1109/ACCESS.2022.3180836.

[32] H. Wang and J. Fei, "Nonsingular terminal sliding mode control for active power filter using recurrent neural network," *IEEE Access*, vol. 6, pp. 67819–67829, 2018.
[33] S. Hochreiter and J. Schmidhuber, "Long short-term memory," *Neural Comput.*, vol. 9, no. 8, pp. 1735–1780, Nov. 1997.
[34] J. Oruh, S. Viriri, and A. Adegun, "Long short-term memory recurrent neural network for automatic speech recognition," *IEEE Access*, vol. 10, pp. 30069–30079, 2022.
[35] Y. Zhou, L. Wang, and J. Qian, "Application of combined models based on empirical mode decomposition, deep learning, and autoregressive integrated moving average model for short-term heating load predictions," *Sustainability*, vol. 14, no. 12, p. 7349, Jun. 2022.
[36] S. R. Mohandes, X. Zhang, and A. Mahdiyar, "A comprehensive review on the application of artificial neural networks in building energy analysis," *Neurocomputing*, vol. 340, pp. 55–75, May 2019.
[37] M. Chang, S. Bae, G. Cha, and J. Yoo, "Aggregated electric vehicle fast-charging power demand analysis and forecast based on LSTM neural network," *Sustainability*, vol. 13, no. 24, p. 13783, Dec. 2021.
[38] K. Ijaz, Z. Hussain, J. Ahmad, S. F. Ali, M. Adnan, and I. Khosa, "A novel temporal feature selection based LSTM model for electrical short-term load forecasting," *IEEE Access*, vol. 10, pp. 82596–82613, 2022.
[39] N. Mamat, F. Yakub, S. A. Z. S. Salim, and M. S. Mat Ali, "Seismic vibration suppression of a building with an adaptive nonsingular terminal sliding mode control," *J. Vibrat. Control*, vol. 26, nos. 23–24, pp. 2136–2147, Dec. 2020.
[40] H. Zhou, A. Che, X. Shuai, and Y. Cao, "Seismic vulnerability assessment model of civil structure using machine learning algorithms: A case study of the 2014 Ms6. 5 Ludian earthquake," *Natural Hazards*, vol. 1, pp. 1–28, Feb. 2014.
[41] S. Li, Z. Zuo, C. Zhai, S. Xu, and L. Xie, "Shaking table test on the collapse process of a three-story reinforced concrete frame structure," *Eng. Struct.*, vol. 118, pp. 156–166, Jul. 2016.
[42] S. S. Madabhushi, J. Hruby, and B. P. Wham, "Experimentally investigating the influence of changing payload stiffness on outer loop iterative learning control strategies with shaking table tests," *J. Vibrat. Control*, vol. 30, nos. 9–10, pp. 1933–1946, May 2024.
[43] S. O. F. Delivery. (2015). *GmbH TIRA Vibration Test Systems TV 50350 / LS-120 GmbH TIRA Vibration Test Systems TV 50350 / LS-120 Vibration Test System TV 50350 / LS-120*.
[44] A. Farzampour and A. K. Asl, "Performance of tuned mass dampers in vibration response control of base-excited structures," *J. Civil, Construct. Environ. Eng.*, vol. 2, no. 3, pp. 87–94, 2017.
[45] D. Vamvatsikos and C. A. Cornell, "Incremental dynamic analysis," *Earth Eng. Struct. Dyn.*, vol. 31, no. 3, pp. 491–514, 2002.

NORMAISHARAH MAMAT received the bachelor's and Master of Science degrees in electrical engineering from Universiti Teknikal Malaysia Melaka and the Doctor of Philosophy degree from Malaysia–Japan International Institute of Technology (MJIIT), Universiti Teknologi Malaysia, Kuala Lumpur, Malaysia. She is currently a Senior Lecturer with the Faculty of Artificial Intelligence (FAI), Universiti Teknologi Malaysia. Her research interests include vibration control, intelligent control, artificial intelligent, and deep learning.

RAWAD ABDULGHAFOR (Member, IEEE) received the bachelor's and master's degrees in computer systems engineering and informatics from Saint Petersburg Electrotechnical University "LETI," Russia, in 2004 and 2007, respectively, and the Ph.D. degree in information technology from International Islamic University Malaysia, Kuala Lumpur, Malaysia, in 2017. He was a Research Assistant with the Faculty of Information and Communication Technology, International Islamic University Malaysia, from 2014 to 2017. He has been an Assistant Professor with the Faculty of Information and Communication Technology, International Islamic University Malaysia, since 2018. He was a Postdoctoral Fellow with Malaysia–Japan International Institute of Technology, Universiti Teknologi Malaysia, Kuala Lumpur, from 2018 to 2019. His research interests include consensus models for multi-agent systems, computation theory, wireless communications, and machine learning.

SHERZOD TURAEV (Member, IEEE) was born in Bukhara, Uzbekistan, in 1973. He received the B.S./M.S. degree in applied mathematics and the Ph.D. degree in mathematics from the National University of Uzbekistan, in 1994 and 2001, respectively, and the Ph.D. degree in computer science from the University of Rovira i Virgili, Tarragona, Spain, in 2010. From 2009 to 2012, he was a Postdoctoral Researcher with the University of Putra Malaysia. From 2012 to 2018, he was an Assistant Professor with International Islamic University Malaysia. Since 2019, he has been an Associate Professor with the Computer Science and Software Engineering Department, College of Information Technology, United Arab Emirates University.

FITRI YAKUB (Senior Member, IEEE) received the Bachelor of Engineering degree in electronic and electrical engineering from Universiti Teknologi Malaysia, the Master of Science degree in electronic and electrical engineering from International University Malaysia, and the Doctor of Engineering degree in automation control from Tokyo Metropolitan University, in 2015. He is currently a Senior Lecturer with Malaysia–Japan International Institute of Technology (MJIIT), Universiti Teknologi Malaysia, Kuala Lumpur, Malaysia. His research interests include intelligent controller, electronic and electrical, vehicle control, and artificial intelligence.

MOHD FAUZI BIN OTHMAN received the B.Math. degree from the University of Wollongong, Australia, in 1900, the M.Eng. (Elect.) degree from Universiti Teknologi Malaysia, Kuala Lumpur, Malaysia, and the Ph.D. degree from The University of Sheffield, Britain, in 2004. He is currently a Professor with the Electronic System Engineering Department (ESE), Malaysia–Japan International Institute of Technology (MJIIT), Universiti Teknologi Malaysia. His research interests include soft computing, intelligent control systems, power system stability, and power system generation scheduling.